A Combined Study of Tc Redox Speciation in Complex Aqueous Systems: Wet-Chemistry, Tc K-/L_3-Edge X-ray Absorption Fine Structure, and Ab Initio Calculations

Kathy Dardenne, Sarah Duckworth, Xavier Gaona, Robert Polly, Bernd Schimmelpfennig, Tim Pruessmann, Jörg Rothe,* Marcus Altmaier, and Horst Geckeis

ABSTRACT: The combination of wet chemistry experiments (measurements of pH, E_h, and [Tc]) and advanced spectroscopic techniques (K and L_3 edge X ray absorption fine structure spectroscopy) confirms the formation of a very stable Tc(V)−gluconate complex under anoxic conditions. In the presence of gluconate and an excess of Sn(II) (at pe + pH ≈ 2), technetium forms a very stable Tc(IV)−gluconate complex significantly enhancing the solubility defined by TcO_2(s) in hyperalkaline gluconate free systems. A new setup for "tender" X ray spectroscopy (spectral range, ∼2−5 keV) in transmission or total fluorescence yield detection mode based on a He flow cell has been developed at the INE Beamline for radionuclide science (KIT light source). This setup allows handling of radioactive specimens with total activities up to one million times the exemption limit. For the first time, Tc L_3 edge measurements (∼2.677 keV) of Tc species in liquid (aqueous) media are reported, clearly outperforming conventional K edge spectroscopy as a tool to differentiate Tc oxidation states and coordination environments. The coupling of L_3 edge X ray absorption near edge spectroscopy measurements and relativistic multireference ab initio methods opens new perspectives in the definition of chemical and thermodynamic models for systems of relevance in the context of nuclear waste disposal, environmental, and pharmaceutical applications.

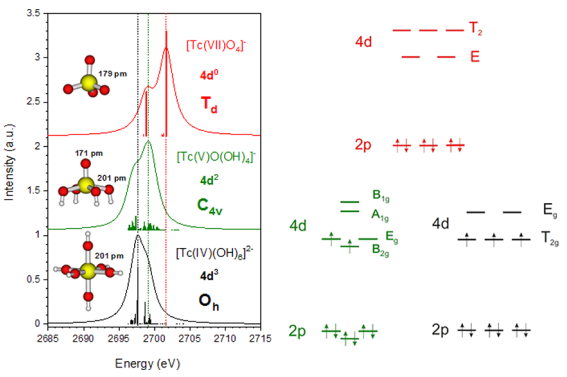

1. INTRODUCTION

^{99}Technetium is one of the main fission products of ^{235}U and ^{239}Pu in nuclear reactors. Due to its long half life ($t_{1/2}$ = 2.121 × 10^5 a) and large inventory in spent nuclear fuel, ^{99}Tc is of great relevance in the context of safety assessment of repositories for radioactive waste. ^{99}Tc is also a relevant contaminant associated with sites for plutonium production or nuclear fuel reprocessing.[1] Among the former, the Hanford site (Washington State, USA) produced nearly 1990 kg of ^{99}Tc (or 1.25 PBq) between 1943 and 1987, which is mainly stored as soluble species in large underground high level waste tanks.[1−3]

A number of the shorter lived isotopes (e.g., ^{95m}Tc with $t_{1/2}$ = 61 days and ^{99m}Tc with $t_{1/2}$ = 6.02 h) are largely used in research applications, especially in the medical field.[1,4] The introduction of a ^{99}Mo/^{99m}Tc generator for clinical applications during the 60s had a significant impact on radiochemistry and nuclear medicine.[4−7]

Technetium has an electron configuration of [Kr] $4d^5 5s^2$ and is characterized by a very rich redox chemistry with reported oxidation states ranging from −I to +VII.[8−11] Oxidation states +IV and +VII are the most stable ones in aqueous systems in the absence of specific complexing ligands. Tc(VII) prevails as the highly soluble and mobile pertechnetate ion (TcO_4^-) in oxidizing to weakly reducing conditions, whereas Tc(IV) forms the sparingly soluble hydrous oxide TcO_2(am, hyd) in strongly reducing conditions as those expected in deep underground repositories for nuclear waste disposal. The thermodynamic description of Tc(IV) solubility, hydrolysis, and complexation with selected inorganic ligands (e.g., carbonate), as well as the redox transition between Tc(VII) and Tc(IV), is well described in the literature, as recently summarized in the critical review work conducted within the NEA TDB project (Grenthe et al., 2020, cf. Supporting Information (SI)). A detailed description of the thermodynamic data currently available for Tc is provided in Section A of the Supporting Information (SI). The importance of Tc(IV) sulfide compounds (mostly as TcS_2 and Tc_2S_7) is reported in the fields of medicine, nuclear waste disposal, or

environmental applications.[12−14] In aqueous systems, the formation of Tc(VI) and Tc(V) is described in a number of electrochemical/polarography studies.[15−19] Because of their involvement in fast disproportionation reactions, both oxidation states are considered unstable in aqueous equili brium systems.[10] The stability of Tc(VI) and Tc(V) is remarkably different in nonaqueous solvents or in the presence of specific coordinating ligands, for which a variety of complexes and solid compounds are reported in the literature.[20−24] Indeed, gluconate complexes of Tc(V) are used as precursors of new Tc complexes by ligand exchange.[4,25,26] Tc(III) is stabilized in acidic reducing conditions,[10,27] with mixed Tc(III,IV) soluble species being reported in very acidic sulfate and chloride solutions.[28,29] Due to the relatively high electron density provided by the d^4 configuration of Tc(III), ligands with back donation capabilities are also reported to stabilize this oxidation state: carbonyl, thiourea, and aminopolycarboxylates (EDTA, NTA, etc.), among others.[24,30,31] Rard and co workers concluded that there is no experimental evidence for the existence of thermodynamically stable Tc(II) in aqueous solution.[10] However, this elusive oxidation state in the aqueous phase can be stabilized in organic solvents in the presence of ligands with sulfur, halogen, and nitrogen donor atoms.[11,32−34] Several nitrosyl and thionitrosyl complexes of Tc(II) are also reported in the literature. Among the latter, Gong and co workers reported the reduction of Tc(VII) by acetohydroxamic acid with the consequent formation of $[Tc^{II}(NO)(AHA)_2(H_2O)]^+$.[35] The formation of this highly soluble complex can have important implications for the UREX reprocessing scheme. A large number of complexes and compounds of Tc(I) are reported in the literature, in many cases containing the carbonyl ligand CO. Tc(I)−CO complexes play an important role in medical applications, with the organometallic semiaqua ion $[Tc(CO)_3(OH_2)_3]^+$ being used as a precursor for the radiolabeling of biomolecules for diagnostic and therapeutic purposes.[4,11,36,37] After several attempts, complexes belonging to the Tc(I)−CO family were also identified in Hanford waste tanks.[38−40] This discovery was challenged by the (expectedly) unfavorable conditions of the waste tanks, e.g., highly alkaline brines under oxidizing conditions. In such environments, hydrolyzed species of the general formula $[Tc(CO)_3(OH_2)_{3-n}(OH)_n]^{1-n}$ expectedly play an important role in the speciation of Tc.[40]

1.1. Characterization of Tc Speciation by XAFS. Tc K edge X ray absorption fine structure (XAFS) spectroscopy—comprising both near edge (XANES) and extended post edge fine structure (EXAFS) investigations—was frequently applied in the past three decades to characterize ^{99}Tc species in solid specimens and liquid phases. Although ^{99}Tc is a radionuclide decaying by β^- emission (~0.3 MeV), its relatively high exemption limit of 1×10^7 Bq renders XAFS measurements with thoroughly encapsulated samples easily feasible at its K absorption edge (E_{1s} (Tc^0), 21.044 keV), even at X ray absorption spectroscopy (XAS) beamline stations that are not specially equipped for radionuclide research (cf. SI Section B for a comprehensive summary).

In contrast to the almost exclusively probed Tc K edge (corresponding to dipole allowed 1s → 5p transitions), excitation of the shallower $2p_{3/2}$ core electrons ($E_{2p3/2}$ (Tc^0), 2.677 keV) probes the unoccupied 4d levels and, depending on the Tc bonding state and symmetry, the corresponding crystal or ligand field splitting (cf. Section 3.3). Note that the core−hole lifetime broadening at the Tc L_3 level is only 1.91 eV compared to 4.91 eV at the K level,[41] enabling detection of subtle spectral differences between different oxidation states and bonding schemes. To the best of our knowledge, up to now (2021), the only publications covering XANES measure ments at the Tc L_3 absorption edge were presented by Blanchard et al. in 2014[42] and Bauters et al. in 2020.[43] In the context of the former study, Tc containing powder samples were embedded in epoxy resin and mounted in a windowless holder. Tc L_3 edge spectra were collected at the Australian Synchrotron using the total electron yield (TEY) and total fluorescence yield (TFY) XAS detection modes with Tc samples held at UHV conditions. In the latter study, a comprehensive series of ^{99}Tc compounds, ranging from oxidation states I to VII, was measured at the Tc L_3 edge applying a new approach to record tender XANES spectra realized at the INE Beamline at the KIT light source,[44] cf. Section 2.4. The new setup is based on a He flow cell, keeping samples at ambient conditions during TFY or transmission XAS data acquisition. As shown below, for the first time, we were also able to collect Tc L_3 edge spectra for liquid ^{99}Tc samples.

2. EXPERIMENTAL AND THEORETICAL METHODS

2.1. Chemicals. All sample preparation and handling were performed in Ar gloveboxes at $T = 22 \pm 2$ °C. All solutions were prepared with purified water (Milli Q academic, Millipore) and purged for 2−3 h with Ar before use to remove traces of O_2 and CO_2. A purified and radiochemically well characterized ^{99}Tc stock solution (1.3 M $NaTcO_4$) was used for the experiments. NaCl (p.a.), $MgCl_2 \cdot 6H_2O$ (p.a.), $Na_2S_2O_4$ (87%), $NaC_6H_{11}O_7$ (NaGLU, ≥99%), HCl Titrisol, and NaOH Titrisol were obtained from Merck. $SnCl_2$ was obtained from Sigma Aldrich.

Caution! ^{99}Tc is a β emitter (E_{max} = 294 keV, $t_{1/2} = 2.1 \times 10^5$ years). All operations were carried out in radiochemical laboratories equipped for handling this isotope.

2.2. pH_m and E_h Measurements. The hydrogen ion concen tration in molal units ($pH_m = -\log[H^+]$) was measured using combination pH electrodes (type ROSS, Orion) calibrated against standard pH buffers (pH 1−12, Merck). The values of pH_m were calculated from the operational "measured" pH_{exp} using empirical corrections factors (A_m), i.e., $pH_m = pH_{exp} + A_m$. The correction factors A_m entailed both the activity coefficient of H^+ and the liquid junction potential of the electrode. A_m values determined as a function of NaCl concentration were previously reported in Altmaier et al.[45]

Redox potentials in redox buffered samples (see Section 2.3) were measured with Pt combination electrodes with a Ag/AgCl reference system (Metrohm) and converted to E_h vs the standard hydrogen electrode by correction for the potential of the Ag/AgCl reference electrode (+207 mV for 3 M KCl at 22 °C). Stable E_h readings were obtained within 10 min in most of the samples. The apparent electron activity ($pe = -\log a_{e^-}$) was calculated from the relation $E_h = -(RT/F) \ln a_{e^-}$, where R is the universal gas constant, T is the temperature (in K), and F is the Faraday constant ($pe = 16.9E_h$ (V) at 25 °C). In the absence of redox couples present in solution in sufficient concentration (above ≈10^{-6} M), measurements of the redox potentials were considered unreliable.[46,47] For this reason, redox potentials of unbuffered samples (see Section 2.3) were not measured and instead assumed to be equal to "redox neutral" conditions. As defined by Neck and co workers,[48] hypothetical partial pressures of $P(H_2(g)) = 2P(O_2(g)) = 2.5 \times 10^{-28}$ bar are calculated for the irreversible reaction $H_2O(l) \Leftrightarrow H_2(g) + 0.5O_2(g)$, which allows calculating the "redox neutral line" as (pe + pH) = 13.8.

2.3. Sample Preparation and Characterization. Two reference samples were prepared for the calibration of Tc L_3 edge XANES. A solution with 20 mM Tc(VII) was prepared by dilution of the $NaTcO_4$ stock solution in 0.1 M HCl. A Tc(IV) reference solid phase

was prepared by electrochemical reduction of a 0.01 M $NaTcO_4$ solution in 1.0 M HCl at $E \approx -50$ mV vs SHE. The resulting suspension was quantitatively precipitated at $pH_m > 12$ in a solution containing 5 mM $Na_2S_2O_4$ as a holding reductant. The solid TcO_2(am, hyd) was aged for six months before use in the present study. These references are quoted as "ref Tc(VII)" and "ref Tc(IV)" in the following sections.

Two additional samples were prepared for the characterization of technetium in the aqueous phase by Tc K and L_3 edge XANES as well as by K edge EXAFS. The effect of gluconate on the redox speciation of Tc in alkaline aqueous solutions was investigated in the absence and presence of a reducing agent, i.e., Sn(II). Gluconate is a polyhydroxocarboxylic acid often used as a superplasticizer in cement formulations, and thus, it is expected under repository conditions. Table 1 summarizes the experimental conditions for the samples investigated in this study (A and B). XANES and EXAFS spectra were collected after an equilibration time of 426 days.

Table 1. Experimental Conditions for the Tc Samples in the Presence of Gluconate Investigated in This Work

sample	$[Tc(VII)]_0$ [M]	$[GLU]_{tot}$ [M]	[NaOH] [M]	redox buffer
A	1×10^{-3}	0.5	0.1	
B	1×10^{-3}	0.5	0.1	0.01 M Sn(II)[a]

[a]Sn(II) is predominantly found as $Sn(OH)_3^-$ in hyperalkaline solutions. This required the titration of the original $SnCl_2$ solution with 3 equiv of NaOH.

Total concentrations of Tc and pH_m were determined in all samples, whereas E_h values were measured for the Tc(IV) reference and for samples A and B. The Tc concentration was quantified by liquid scintillation counting (LSC, Quantulus, PerkinElmer) after 10 kD ultrafiltration (2−3 nm, Pall Life Sciences) and mixing with 10 mL of an LSC cocktail (Ultima Gold XR, PerkinElmer).

2.4. Experimental Setup for Tc K- and L_3-Edge XAFS Measurements. Tc K edge XAFS spectra were collected at the KIT light source (KARA storage ring, KIT Campus North), either using the conventional TFY XAS setup at the INE Beamline[44] or at the ACT station of the CAT ACT beamline.[49] Both beamlines are equipped to handle radioactive samples with total activities up to 1×10^6 times the European exemption limit, adhering to a redundant but flexible containment protocol easily adaptable to the specific type of sample system or process under investigation. Tc K edge spectra were recorded by detecting the Tc Kα line using a 5 pixel LEGe solid state detector (Canberra, Belgium), using an Ar filled ionization chamber (Poikat, Germany) at ambient pressure as the I_0 monitor. The double crystal monochromators (DCM) were equipped with a pair of Ge⟨422⟩ and a pair of Si⟨311⟩ crystals at the INE Beamline and CAT ACT, respectively. In both cases, the energy scale was calibrated by assigning the first inflection point in the rising K edge absorption of Mo metal foil (20 μm) to the 1s energy (E_{1s} (Mo^0), 20.0 keV). All Tc samples were measured in sealed polyethylene vials held in an Ar flushed inert gas transfer cell.

A new setup for tender X ray measurements at the INE Beamline (currently applicable down to the phosphorus K edge at ∼2.14 keV) was developed and initially tested at the S K and Mo L_3 edges (∼2.47 and ∼2.52 keV, respectively). The system was based on a He flow cell comprising a first ionization chamber (Oken, Japan, 5 cm length), bellows, a sample chamber, bellows, and a second ionization chamber (Oken, Japan, 19 cm)—all connected without intersecting windows (Figure 1). The first ionization chamber (IC) was directly flanged to the adapter plate holding the beamline exit window (25 μm KAPTON). The sample chamber was mounted at a linear table on top of the multiaxis sample positioning stage (Huber, Germany), allowing its lateral and vertical translation each by ±6 mm. The second IC was rigidly mounted at the X 95 rail carrying the downstream ionization chambers for conventional high energy XAS measurements. A He flow of 1 L/min (inlet at the second IC, outlet at the first IC, exhausted via the ventilation system of the experimental hutch) was provided to constantly purge the chamber arrangement. The sample chamber was manufactured as a transparent acrylic glass cube equipped with ISO KF40 entrance and exit flanges and a sealed lid at the top, which can be opened to introduce various types of sample cells, vials, or holders. The major technical challenge was to position the Be entrance window of the solid state detector for TFY measurements (Vortex 60EX, Hitachi, USA) close to the sample surface without directly exposing the detector snout to the He atmosphere in the sample chamber. This was solved by fitting the right hand side (in the beam direction) of the sample chamber with a sealed KAPTON window (13 μm) on a frame protruding 20 mm into the chamber volume, cf. the inset to Figure 1. The racetrack shape of the frame allowed vertical sample positioning scans of the cell with an inserted detector, while lateral positioning scans (at 90° relative to the impinging beam) were coupled to synchronous movements of the lateral detector positioning stage, keeping the sample to Be window distance constant. Intensity losses due to the absorption of Tc Lα

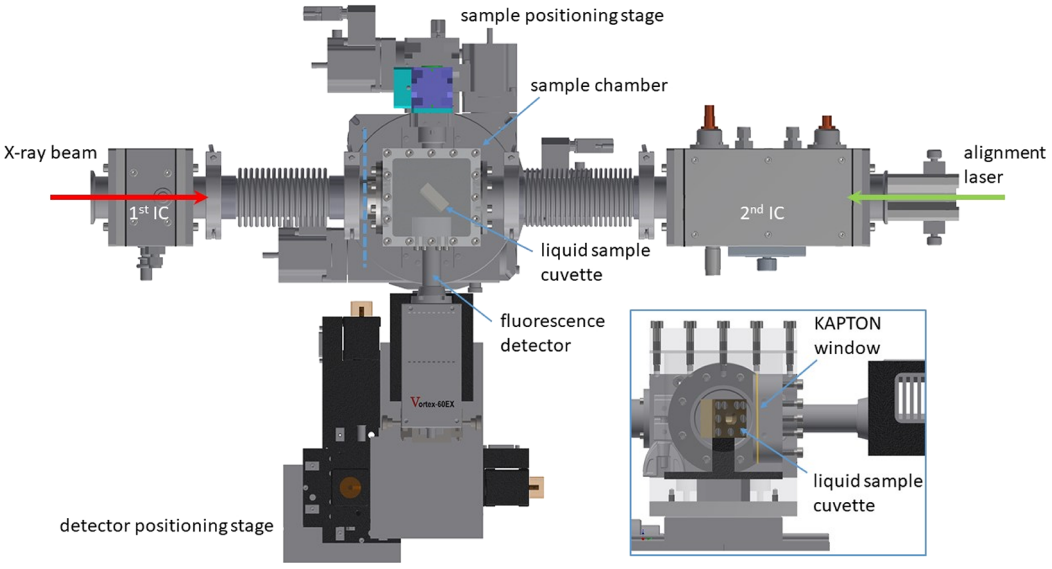

Figure 1. Top view of the He flow cell for tender XAFS measurements of radioactive samples including liquids, cf. the text for a detailed description of all components. The inset (bottom right) depicts a cross sectional view in the X ray beam direction across the dashed blue line.

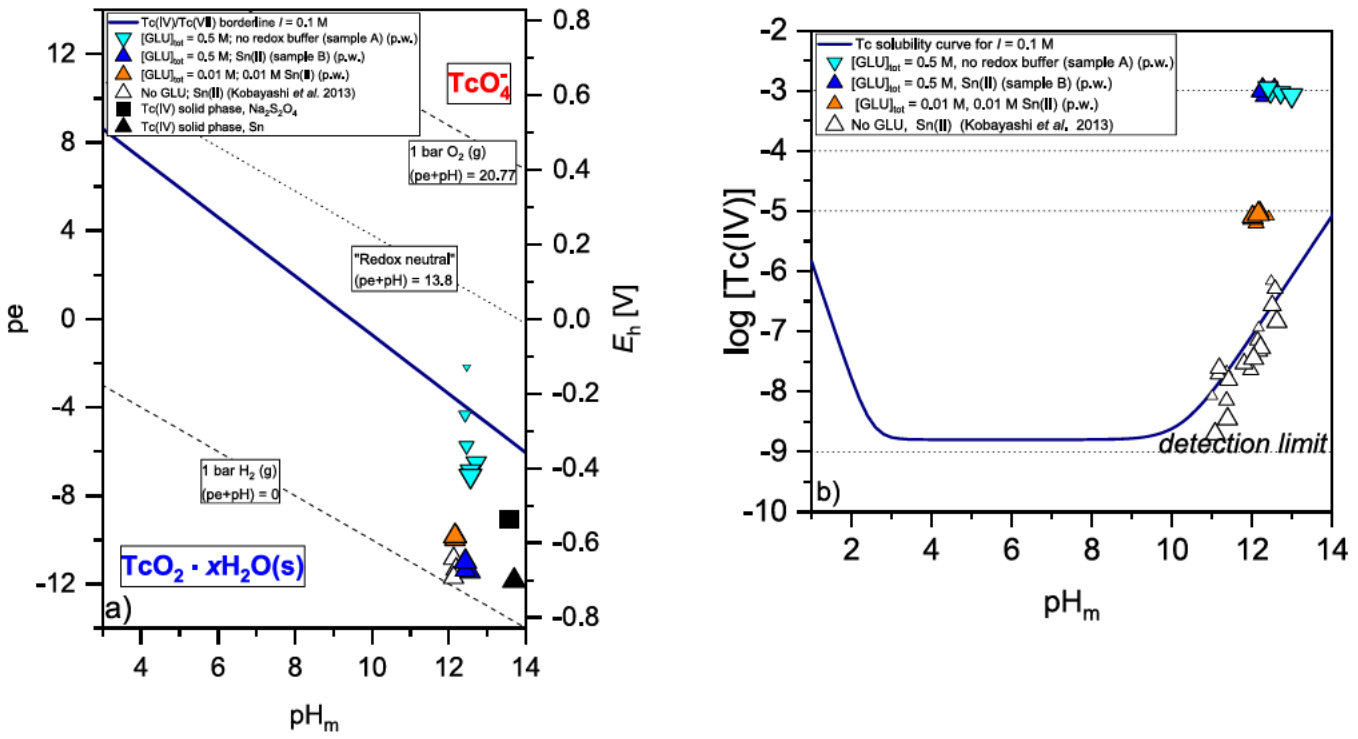

Figure 2. (a) Pourbaix diagram of Tc calculated for $1 \leq pH_m \leq 13$ and $-14 \leq pe \leq 14$ in 0.1 M HCl–NaCl–NaOH solutions. Symbols correspond to experimental ($pe + pH_m$) values for reference Tc(VII), reference Tc(IV) (TcO_2(am, hyd)), and samples A and B. The ($pe + pH_m$) values of reference Tc(VII) and sample A (both redox unbuffered) are assigned to the redox neutral line (see the text). (b) Solubility curves of TcO_2(am, hyd) calculated for 0.1 M HCl–NaCl–NaOH solutions. Symbols correspond to the experimentally measured [Tc] as determined in this work or reported by Kobayashi et al. (2013). All calculations were performed including thermodynamic data selected in ref 27 and reported in ref 74.

fluorescence (~2.42 keV) in the KAPTON window and the remaining air gap amounted to ~30%.

Standard samples (such as thin films or powders dusted to adhesive tape) were attached to a stand inside the sample chamber held in position by magnets on a metallic base plate. Radioactive liquids such as ^{99}Tc containing solutions investigated in this work were filled in PEEK (polyether ether ketone) cuvettes sealed by KAPTON films as recently developed by Vitova et al. at KIT INE for actinide M edge high energy resolution X ray emission spectroscopy (HR XES).[50] Coarse positioning of the samples was accomplished with the help of a class 3B alignment laser entering via the exit window of the second IC and pointing to the X ray beam spot at the sample position. Fine positioning relies on X ray fluorescence intensity profiles.

Using the setup described above, Tc L_3 edge XAFS spectra were recorded in TFY mode detecting the Tc Lα line, using the He flushed first IC as the I_0 monitor. The DCM was equipped with a pair of Si⟨111⟩ crystals. The energy scale was calibrated by assigning the white line (sulfate) peak maximum in the sulfur K edge spectrum of Na_2SO_4 to 2.477 keV, which was in turn calibrated against the 1s → 4p Rydberg transition of Ar (3.20354 keV).[51] PEEK cuvettes with 13 μm KAPTON windows were placed in the sample chamber with the surface of the window at 45° relative to the impinging beam.

2.5. Relativistic Multireference Ab Initio Study of Tc L_3-Edge XANES Spectra. During the past decades, relativistic multireference ab initio quantum chemistry methods have developed into a powerful tool supporting X ray spectroscopy techniques.[52−54] Because of the complexity of the detected signals, theoretical calculations are mandatory for the interpretation of the experimental data. For recent extensive reviews, see, e.g., refs 55−57.

2.5.1. Structures of the Different Tc Species: $[Tc(VII)O_4]^-$, $[Tc(V)O(OH)_4]^-$, $[Tc(IV)(GLU_{-2H})_2(OH)_2]^{4-}$, and $[Tc(OH)_6]^{2-}$. A prerequisite for the calculation of the XANES spectra of the different Tc compounds investigated in this study is reliable structures. We optimized structures of the different $[Tc(VII)O_4]^-$, $[Tc(V)O(OH)_4]^-$, $[Tc(IV)(GLU_{-2H})_2(OH)_2]^{4-}$, and $[Tc(IV)(OH)_6]^{2-}$ species with TURBOMOLE (www.turbomole.com)[58−63] on the RI DFT level using the def2 TZVP[64−66] basis set. Except for $[Tc(VII)O_4]^-$, all other species were taken as idealized structures aiming at reproducing the yet unknown structures of the Tc–gluconate complexes investigated in this work.

2.5.2. Tc L_3-Edge XANES Calculations. We tackled the calculation of the Tc L_3 edge XANES spectra (corresponding to $2p_{3/2} \rightarrow 4d_{3/2,5/2}$ excitations) of the different Tc moieties applying relativistic multireference ab initio methods available in MOLCAS8.4.[67] We used the restricted active space (RASSCF) method[68] and for the inclusion of the dynamical correlation second order perturbation theory RASPT2[69] with an IPEA shift of 0.0. Spin–orbit interactions were calculated in the restricted active space state interaction (RASSI) scheme.[70] For the RASSCF/RASPT2 calculations, we subdivided the active space. The RAS1 space contains the core states (2p), and the 4d orbitals are in the RAS2/3 space. In total, we had 6 ($[Tc(VII)O_4]^-$), 8 ($[Tc(V)O(OH)_4]^-$), and 9 ($[Tc(IV)(OH)_6]^{2-}$) active electrons distributed in the active space. There were no restrictions on the number of electrons in RAS1 for the ground state calculations, but for the excited state calculations, the RAS1 space was restricted to contain only 5 electrons. Both scalar relativistic and spin–orbit coupling were accounted for in our calculations. For the spin–orbit interaction calculations, all relevant spin states were included in the calculations. As basis sets, we used the ANO basis sets[71,72] available in MOLCAS. We performed the calculations using the full t_d $[Tc(VII)O_4]^-$, C_{4v} $[Tc(V)O(OH)_4]^-$, and O_h $[Tc(IV)(OH)_6]^{2-}$ symmetry with the SUPERSYMMETRY option imposing higher supersymmetry by restricting rotations to irreducible representations in the RASSCF calculations. Experimental spectra were simulated by applying a Lorentzian profile at the calculated transition energies with the intensities given by the oscillator strengths with a full width at half maximum γ of 1.2–2.5 for the different species.

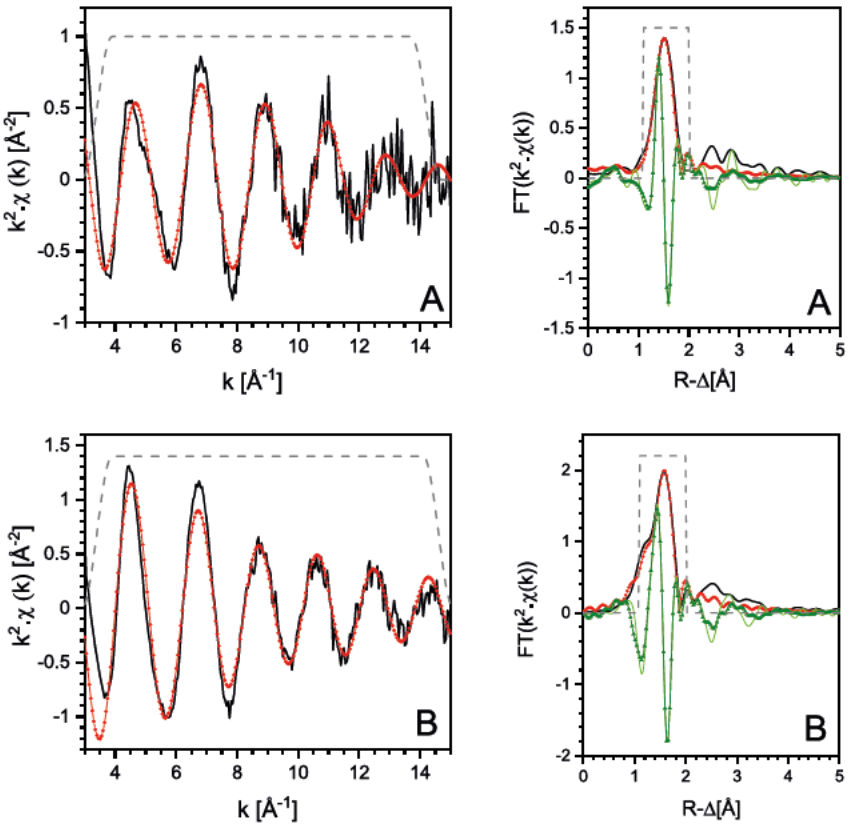

Figure 3. Tc K edge EXAFS spectra of sample A (top) and sample B (bottom): left panels, k^2 weighted $\chi(k)$ (black solid line) and fit (red line with filled circles); right panels, Fourier transform (FT) magnitude and imaginary part of k^2 weighted $\chi(k)$ (black and light green solid lines, respectively) and corresponding R space fit results (red line with filled circles and dark green line with filled triangles, respectively). Windows for forward FT and the fit range are indicated by dashed lines.

3. RESULTS AND DISCUSSION

3.1. Standard Characterization of the Tc Samples.

Figure 2a shows the Pourbaix diagram of Tc calculated for 0.1 M NaCl−NaOH solutions, including also the experimental or calculated (pe + pH_m) values for the reference Tc(VII), reference TcO_2(am, hyd), and samples A and B. Figure 2b shows the solubility curve of TcO_2(am, hyd) calculated for 0.1 M NaCl, including the experimental log[Tc] measured for the same systems as in Figure 2a. For comparative purposes, Figure 2b includes also experimental data reported by Kobayashi et al. under analogous experimental conditions (oversaturation experiments with Tc(VII), use of Sn(II) as a reducing chemical) but in the absence of gluconate.[73]

Figure 2a shows that strongly reducing (pe + pH_m) conditions are measured in those systems containing $Na_2S_2O_4$ or Sn(II) (reference Tc(IV) and sample B). These values of (pe + pH_m) are in line with previous studies reporting the use of $Na_2S_2O_4$ and Sn(II) in the presence of Tc.[73,75,76] In these samples and according to thermodynamic calculations shown in Figure 2a, Tc is expected in the +IV oxidation state. The values of pe in the redox unbuffered sample A are assigned to the redox borderline and thus fall within the stability field of Tc(VII). Note, however, that no thermodynamic data are available for the interaction of Tc with gluconate. As discussed in the Introduction and in Section A of the SI, the presence of this organic ligand may increase the stability field of Tc(IV) or promote the stabilization of intermediate oxidation states of Tc (e.g., +V), accordingly affecting the Pourbaix diagrams for samples A and B.

The concentration of Tc in samples A and B remained constant (≈10^{-3} M) within the time frame of this study (426 days). Additional samples prepared under analogous conditions (Sn(II), presence of gluconate) but with lower initial Tc(VII) concentration (≈10^{-5} M; orange symbols in Figure 2; samples not characterized by XAFS techniques in this work) did not show any decrease in the Tc concentration either. According to thermodynamic calculations and (pe + pH_m) values plotted in Figure 2a, Tc is expected to precipitate as TcO_2(am, hyd) in sample B thus resulting in a clear decrease in the initial concentration of Tc, which is not observed experimentally. Note further that analogous experiments conducted by Kobayashi et al. in the absence of gluconate resulted in a clear decrease in the initial Tc concentration within 130 days (white triangles in Figure 2b).[73] This comparison provides indirect evidence of the key role of gluconate in the redox phenomena of Tc in alkaline reducing systems.

3.2. Characterization of the Tc Samples by Tc K- and Tc L_3-Edge XAFS.

3.2.1. Tc K-Edge XAFS. Tc K edge EXAFS spectra of Tc−gluconate samples A and B and the corresponding R space fit results are depicted in Figure 3. Table 2 shows that two oxygen shells are required to reproduce the EXAFS spectra of sample A, corresponding to the Tc(VII) sample equilibrated in the presence of gluconate and the absence of Sn(II). Distances Tc−O_1 and Tc−O_2 are in line with reported data for Tc(V) compounds with organic oxo ligands, e.g., Tc(V) diolate or Tc(V) oxalate. A large group of ligands with O, N, S, As, or P donors are known to stabilize

Table 2. Structural Parameters Obtained in This Work from the EXAFS Evaluation of Samples A and B, Together with Structural Information Reported in the Literature for Tc(IV) and Tc(V) Complexes with Organic Oxo Ligands[a]

sample description/reference	path	CN	R (Å)	σ^2 (Å^2)	ΔE_0 (eV)	R-factor
sample A/this work	Tc O_1	1*	1.64	0.0013	2.27	0.017
	Tc O_2	4.4	1.97	0.0017		
sample B/this work	Tc O	6.0	2.01	0.0012	2.27	0.015
Tc(VII) ref/this work	Tc O	4*	1.72	0.0012	4.11	0.014
"Tc(IV) gluconate"/Lukens et al. (2004)[39]	Tc O	6*	2.01(1)	0.0045(1)	5.2(3)	
		6*	3.37(2)	0.015(3)		
"Tc(IV)-oxalate", $[AsPh_4]_2[Tc(ox)_3]$/Colmanet et al. (1987)[77]	Tc O_1	2	1.978(5)			
	Tc O_2	2	1.990(5)			
	Tc O_3	2	2.001(4)			
"Tc(IV)-EDTA", $(H_2EDTA)Tc(\mu\text{-}O)_2Tc(H_2EDTA)\ 5H_2O$/Buergi et al. (1981)[78]	Tc O_1	1	1.923(5)			
	Tc O_2	1	1.907(5)			
	Tc O_3	1	2.007(5)			
	Tc O_4	1	2.020(5)			
	Tc N_1	1	2.190(6)			
	Tc N_2	1	2.198(7)			
"Tc(V)-diolate", $(n\text{-}Bu_4N)[TcO(O_2C_6H_4)_2]$/Davison et al. (1987)[79]	Tc O_1	1	1.648(5)			
	Tc O_2	2	1.956(3)			
	Tc O_3	2	1.958(3)			
"Tc(V)-oxalate", $[AsPh_4]_2[TcO(ox)_2(Hox)]\ 3H_2O$/Baldas et al. (1988)[80]	Tc O_1	1	1.640(6)			
	Tc O_2	1	1.966(7)			
	Tc O_3	1	2.014(6)			
	Tc O_4	1	2.031(6)			
	Tc O_5	1	2.052(7)			
	Tc O_6	1	2.069(6)			
Structures optimized by DFT						
$Tc(VII)O_4^-$	Tc O	4	1.79			
$[Tc(V)O(OH)_4]^-$	Tc O_1	1	1.71			
	Tc O_2	4	2.01			
$[Tc(IV)(OH)_6]^{2-}$	Tc O	6	2.01			
$[Tc(IV)(GLU_{-2H})_2(OH)_2]^{4-}$	Tc O_1	2	1.99			
	Tc O_2	4	2.07			
Average			2.04			

[a]Fit errors: CN, ±20%; R, 0.01 Å; σ^2, 0.0006 Å^2. *Held constant during the fit. Distances Tc−O obtained from the structures optimized by DFT are appended for comparison.

Tc(V).[24] In these complexes, the distance Tc−O in the $[Tc{=}O]^{3+}$ core is reported to range between 1.61 and 1.68 Å. Our experimental observations in combination with data available in the literature underpin the reduction of Tc(VII) with the consequent formation of a Tc(V)−gluconate complex in solution.

A single Tc−O shell with CN = 6.0 ± 1.2 and R_{Tc-O} = 2.01 ± 0.01 Å properly explains the EXAFS spectra collected for Tc(VII) equilibrated with Sn(II) and gluconate (sample B). These structural parameters are in excellent agreement with data previously reported by Lukens and co workers for the complex $Tc(IV)(GLU_{-2H})_2^{2-}$, where "GLU_{-2H}" is the gluconate ligand with two deprotonated alcohol groups.[39a] Analogously to the present study, the Tc(IV)−gluconate complex reported by Lukens and co workers was prepared in alkaline conditions (1 M NaOH) by reducing Tc(VII) with a large excess of $Na_2S_2O_4$ in the presence of $[GLU]_{tot}$ = 0.1 M.

Single crystal analyses of other complexes of Tc(IV) with oxo ligands report also coordination numbers of 6 with analogous Tc−O distances (see Table 2). All these pieces of evidence unequivocally support the predominance of a Tc(IV)−gluconate complex in sample B.

There is ample evidence in the literature reporting the use of Sn(II) for the preparation of Tc(V)−gluconate complexes from Tc(VII) in acidic to hyperalkaline pH conditions.[25,81−84] However, most of these studies were conducted at short equilibration times (or often, time is not reported in the experimental description), and thus, the authors may have missed the evolution of the system at longer contact times. For the reduction of Tc(VII) by Sn(II) in citrate media, Steigman and co workers reported the predominance of a Tc(V)−citrate complex at short equilibration times (≈ minutes), which evolved toward the full conversion to a Tc(IV)−citrate complex at longer contact times (≈ hours).[85] This is in line with our observations for the Tc−gluconate system in Sn(II) media at very long equilibration times (t > 400 days).

Figure 4 depicts the normalized Tc K edge XANES spectra (vertically shifted for clarity) together with those of amorphous $Tc(IV)O_2{\cdot}xH_2O(am)$ and aqueous $Tc(VII)O_4^-$ reference samples (ref Tc(IV) and ref Tc(VII), respectively). Additionally, the spectrum of the complex $Tc^{IV}(GLU_{-2H})_2^{2-}$, reproduced from Lukens et al.,[39] and the spectrum of the tetrabutylammonium (TBA) polyoxometalate cluster $TBA_4[Tc^{V}O\ PW_{11}O_{39}]$, reproduced from Burton Pye et al.,[86] are plotted for comparison. The spectra of sample A, presumably a Tc(V)−gluconate complex, and that of the polyoxometalate stabilized Tc(V) reported by Burton Pye et al. coincide well with the presence of a pre edge feature at around

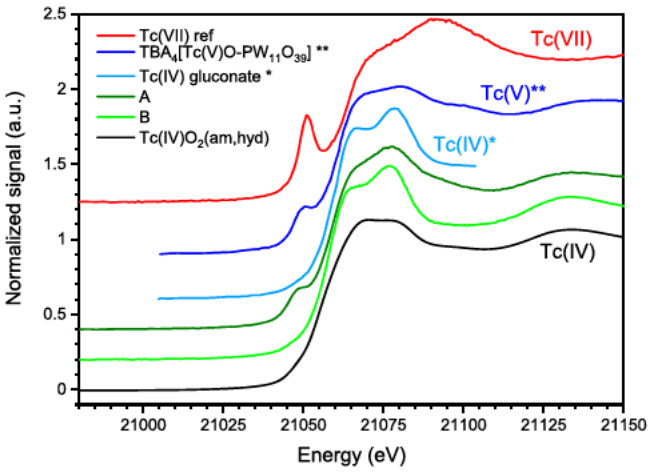

Figure 4. Normalized Tc K edge XANES spectra of gluconate samples A and B and reference compounds (spectra are vertically shifted for clarity). *Data and **data recalibrated via the $(TcO_4)^-$ pre edge peak maximum. *Data reproduced from ref 39. Copyright 2004 American Chemical Society. **Data reproduced with kind permission from ref 86. Copyright 2019 John Wiley and Sons.

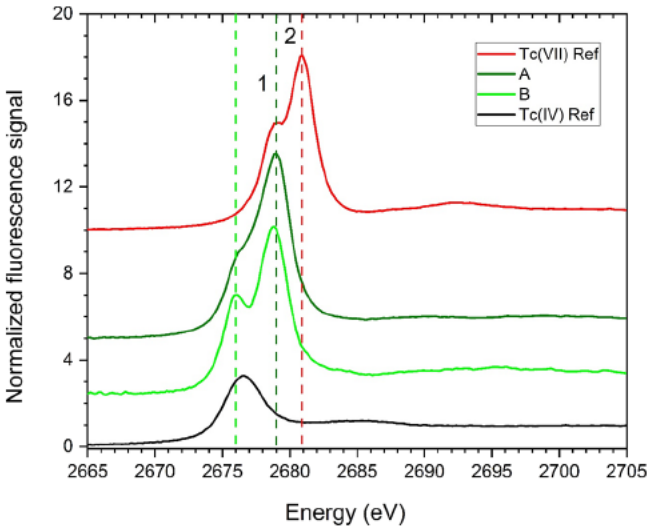

Figure 5. Normalized Tc L_3 edge XANES spectra of gluconate samples A and B and reference compounds (spectra are vertically shifted for clarity, vertical dashed lines to guide the eyes to peak 1 and peak 2 positions).

21.048 keV and the similarity of the featureless edge crest region beyond 21.067 keV, both reflecting the distorted square pyramidal coordination geometry adopted by the Tc(V)=O (C_{4v}) moiety. This observation is in excellent agreement with the corresponding EXAFS fit results obtained for the Tc coordination environment of sample A (cf. Table 2). Likewise, the Tc K edge XANES spectrum of sample B matches that of $Tc(IV)(GLU_{-2H})_2^{2-}$, reflecting the octahedral coordination geometry (O_h) of the tetravalent Tc cation in both gluconate complexes and the TcO_2 reference. Again, this interpretation is corroborated by our Tc K edge EXAFS results. Generally, K edge XANES features of the 4d transition metal Tc ($5s^24d^5$) reflect the probability of dipole allowed Tc 1s → 5p transitions. As shown in the Introduction, the technique has been mostly employed to differentiate heptavalent and tetravalent Tc species or their mixtures. This fingerprinting is based on the appearance of the characteristic pre edge transition feature in the case of the pertechnetate moiety, where the absence of inversion (O_h) symmetry (as in the octahedral Tc(IV) species) allows the hybridization of metal 4d and 5p states. Note that to a lesser extent, such a feature is also visible in the case of the square pyramidal Tc(V) coordination. As pointed out by Blanchard et al.,[42] the 1s electron in Tc K edge XANES is only probing the p type character of the hybridized unoccupied states; thus, the technique does not provide direct access to the crystal field dependent splitting of the 4d manifold.

3.2.2. Tc L_3-Edge XANES. In contrast to Tc K edge XANES, dipole allowed transitions of the $2p_{3/2}$ electrons excited at the Tc L_3 edge directly probe the lowest energy, unoccupied 4d states. Additionally, a significantly increased energy resolution due to the reduced core−hole lifetime broadening provides greater sensitivity to changes in the local Tc coordination geometry as demonstrated by Blanchard et al. in their pioneering L_3 edge XANES study.[42] Figure 5 depicts the Tc L_3 edge XANES spectra of samples A and B together with the liquid pertechnetate (ref Tc(VII)) and the amorphous $TcO_2{\cdot}xH_2O$(am) reference (vertically shifted for clarity). Note that to the best of our knowledge, the spectra of samples A and B and the $Tc(VII)O_4^-$ solution are the first Tc L_3 edge spectra reported in the literature, which have been obtained for liquid (aqueous solution) samples. Pertechnetate and samples A and B exhibit a splitting of the most intense transition feature (white line, WL). In contrast to that, the WL observed for TcO_2 is more symmetric and less intense. The latter observation has to be attributed to the higher filling of the 4d states in TcO_2 (d^3) but might be as well affected by "self absorption" when recording the Tc Lα fluorescence from a concentrated bulk sample. The spectra have been further analyzed by fitting two pseudo Voigt functions (called peak 1 and peak 2) and an arc tangent function (representing the continuum transition above the edge). Fit results (positions of peaks 1 and 2, the center of mass of peaks 1 and 2, and the energy differences between peak 2 and peak 1) are plotted in Figure 6. As expected, the center of mass and the energy positions of peaks 1 and 2 monotonously increase with the formal Tc oxidation state, a well known phenomenon for transition metal XANES spectra due to the decreasing screening of the nuclear charge. Interestingly, the WL splitting

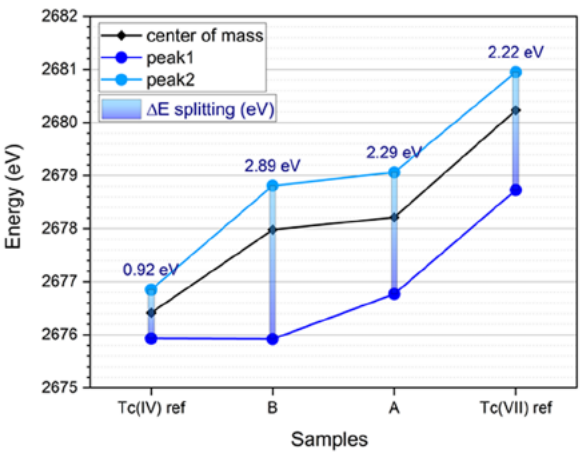

Figure 6. White line peak positions and energy splitting extracted by peak fitting of Tc L_3 edge XANES spectra depicted in Figure 5 (see the text for details).

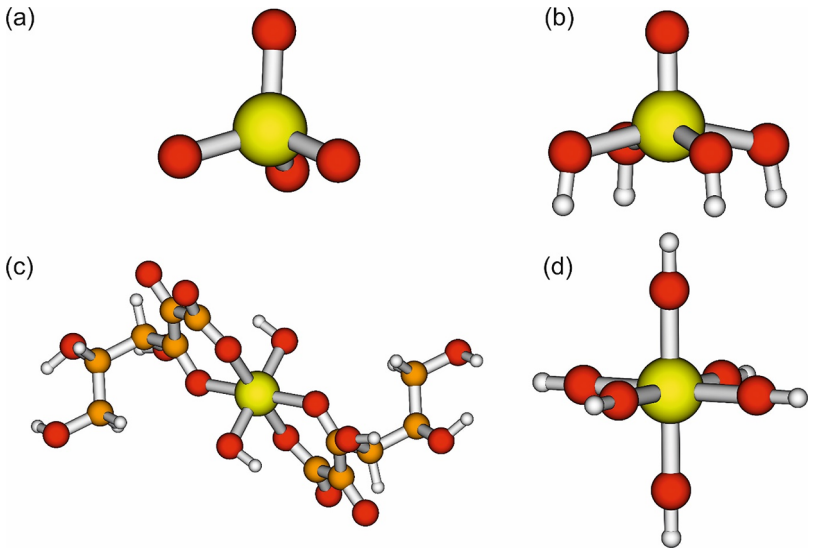

Figure 7. DFT optimized structures for (a) tetrahedral pertechnetate $[Tc(VII)O_4]^-$, (b) square pyramidal $[Tc(V)O(OH)_4]^-$, (c) $[Tc(IV)(GLU_{-2H})_2(OH)_2]^{4-}$ (C_i symmetry), and (d) octahedral $[Tc(IV)(OH)_6]^{2}$.

exhibits the highest value for sample B (Tc(IV)−gluconate) and decreases via sample A (Tc(V)−gluconate) to pertechnetate. Generally, peaks 1 and 2 in L_3 edge XANES spectra of 4d transition metals are associated with transitions to unoccupied, crystal field split 4d levels (cf. ref 42 and references therein and Section 3.3.2), denoted according to the irreducible representations of the corresponding symmetry groups. This energy splitting depends on the ligand field strength, which typically increases as the oxidation state increases (with similar bond distances) or the bond length decreases. Thus, one might assume that the decreased Tc−O bond length observed for sample B compared to $TcO_2{\cdot}xH_2O(am)$[87] explains the distinct energy splitting of the former Tc(IV) species. As shown below (Section 3.3), attempts for DFT optimizations of the coordination polyhedron of sample B as a basis for ab initio calculations of the corresponding Tc L_3 edge XANES spectra, as for now, have not been successful. Note that Bauters et al.[43] reported a remarkable range of the WL shape and crystal field splitting for various Tc(IV) complexes in their recent comprehensive Tc L_3 edge XANES study of technetium oxidation state signatures depending on the ligand type and the coordination structure.

3.3. Relativistic Multireference Ab Initio Calculations of the Tc L_3-Edge XANES Spectra. *3.3.1. Structures of the Different Tc Species: $[Tc(VII)O_4]^-$, $[Tc(V)O(OH)_4]^-$, $[Tc(IV)(GLU_{-2H})_2(OH)_2]^{4-}$, and $[Tc(IV)(OH)_6]^{2-}$.* For all the relevant Tc species with different oxidation states, either a molecule or a suitable model system was optimized without considering any hydration shell. As shown below in Subsection Section 3.3.2, all considered species have single reference ground states, and therefore, DFT can be applied. The optimized structures are shown in Figure 7, and the optimized bond lengths are included in Table 2.

The pertechnetate ion $[Tc(VII)O_4]^-$ has a well defined tetrahedral structure (Figure 7a), which we optimized by DFT. The Tc−O bond distances are 179 pm, which compares very well with the available experimental data.[88] For the Tc(V) species, the situation is quite different. The initial guess for the Tc(V) structure in sample A was based on the Tc coordination suggested by Davison et al.[79] (cf. Figure 1 therein). Motivated by their structure, we optimized a pyramidal $[Tc(V)O(OH)_4]^-$ cluster in C_{4v} symmetry (Figure 7b). The four dangling bonds at the oxygen atoms were saturated with hydrogen atoms. The two Tc−O bond lengths are 171 and 201 pm. The results agree very well with the experimental data (see Table 2) of 164 and 197 pm. For the solid TcO_2(s), we optimized a $[Tc(IV)(OH)_6]^{2-}$ model system (Figure 7d) in O_h symmetry and saturated the dangling oxygen bonds with hydrogen atoms. The corresponding Tc−O bonds are with 201 pm very close to the experimental results for Tc(IV) complexes, e.g., Tc(IV) oxalate listed in Table 2 (199 pm average Tc−O distance). For the structure of the Tc(IV)−gluconate complex, a model comprising two $(OH)^-$ and two $(GLU_{-2H})^{3-}$ moieties was assumed considering the structure suggested by Lukens et al.[39] The corresponding Tc K edge XANES (sample B) spectrum lacks a 1s → 4d/5p pre edge feature, thus pointing to inversion symmetry in this structure (cf. Section 3.2.1). Accordingly, we optimized the $[Tc(IV)(GLU_{-2H})_2(OH)_2]^{4-}$ structure in C_i symmetry (see Figure 7c). The oxygen atoms forming bonds to Tc are in an arrangement resembling very closely the octahedral symmetry. The corresponding bond lengths are 199 pm for Tc−O(H^-) and 207 pm for Tc−O(COH^-). Both average to 204 pm. The inclusion of additional water molecules in the optimization leads to only small changes: 203 pm for Tc−O(H^-) and 204 pm for Tc−O(COH^-) (average of 204 pm). Hence, in this case, the experimental results of 201 pm obtained in this work and by Lukens et al. for Tc(IV)−gluconate (Table 2) are also very well reproduced.

3.3.2. Calculations of the Tc L_3-Edge XANES Spectra. For all the structures considered here, we placed the Tc ion at the origin. For the $Tc(VII)O_4^-$ tetrahedron and the $Tc(IV)(OH)_6^{2-}$ octahedron, one Tc−O bond is oriented along the z axis. For the $Tc(V)O(OH)_4^-$ complex, the short Tc−O bond is oriented along the z axis, and the other four oxygen atoms are aligned with the x and y axes. This is important to have a unique designation of all the 4d orbitals in the different calculations.

The ground states of the considered species have either an empty 4d shell ($Tc(VII)O_4^-$, $S = 0$) or a partially filled 4d shell ($[Tc(V)O(OH)_4]^-$: $4d_{xy}^{1}4d_{xz}^{1}$, $4d_{xy}^{1}4d_{yz}^{1}$, $S = 1$; $[Tc(IV)(OH)_6]^{2-}$: $4d_{xy}^{1}4d_{xz}^{1}4d_{yz}^{1}$, $S = 3/2$). The RASSCF

calculations show that they are all single reference states, which allow DFT optimization of the ground state structure. The presence of 2 or 3 electrons in the 4d shell for the Tc(V) and Tc(IV) cases leads to contributions of transitions from the ground state to many excited states to the L_3 edge XANES spectra: for $Tc(VII)O_4^-$, there are 40, for $[Tc(V)O(OH)_4]^-$ 479, and for $[Tc(IV)(OH)_6]^{2-}$ 871 states.

We determined the excitation energies corresponding to the Tc L_3 edge XANES spectrum of TcO_4^- with the ANO VDZ/VTZ/VQZ basis sets. The results are summarized in Table 3.

Table 3. Tc L_3 Edge XANES Excitation Energies of TcO_4^- [a]

method	basis set	E_1	E_2	$\Delta E = E_2$	E_1
exp.		2678.7	2680.9	2.2	
RASSCF	ANO-VDZ	2702.8	2705.7	2.9	
RASPT2		2698.7	2700.2	1.5	
RASSCF	ANO-VTZ	2698.9	2701.7	2.8	
RASPT2		2694.0	2695.5	1.5	
RASSCF	ANO-VQZ	2694.8	2697.7	2.9	
RASPT2		2689.9	2691.4	1.5	

[a]Comparison of calculated and experimental results. All energies are in eV.

Both RASSCF and RASPT2 results are similar and in good agreement with experimental data. The RASPT2/ANO VQZ results (transition energies and scaled oscillator strengths) are shown in the right panel of Figure 9.

Due to the ligand field splitting of the d orbitals in the tetrahedron, there are two lower lying states in the irreducible representation E of t_d and three higher lying states in T_2. The two peaks visible in the spectrum (denoted as 1 and 2 in Table 3 and in Figure 5) can be assigned to excitations from $2p_{3/2} \rightarrow 4d_{xz}/4d_{x2-y2}$, $4d_{yz}/4d_{xy}$ (2678.7 eV, all 4d orbitals in E) and $2p_{3/2} \rightarrow 4d_{yz}/4d_{xy}$, $4d_{xz}/4d_{x2-y2}$, $4d_{z2}$ (2680.9 eV, all 4d orbitals in T_2). The excited states are predominantly singlet states ($S = 0$) with a small admixture of triplet states ($S = 1$). Due to the orientation of one TcO bond along the z axis, the 4d orbitals mix strongly. The improvement of the results increasing the basis set from ANO VDZ to ANO VQZ can be clearly seen. The energy shift compared to the experimental spectra is significantly reduced with increasing basis set size. For all applied basis sets, the RASPT2 results are closer to the experiment than the corresponding RASSCF result. The splitting between the two peaks is ~2.8−2.9 eV for the RASSCF calculations and ~1.5 eV for the RASPT2 calculations. Therefore, the RASPT2 results are in slightly better agreement with the experiment than the RASSCF results. It can be seen from Figure 9 that the Tc L_3 edge XANES spectrum of $[Tc(VII)O_4]^-$ consists only of a few transitions.

For the calculations on $[Tc(V)O(OH)_4]^-$, $[Tc(IV)(OH)_6]^{2-}$, and $[Tc(IV)(GLU_{-2H})_2(OH)_2]^{4-}$, we applied only the RASSCF method with the ANO VTZ basis set due to the very large number of involved excited states. The Tc L_3 edge XANES spectrum of $[Tc(V)O(OH)_4]^-$ clearly shows two main peaks. The splitting of the 4d states in this pyramidal structure is similar to that in the octahedral ligand field (Figure 8). The 4d orbitals form two groups. In the first group are three 4d orbitals (irreducible representation E_g and B_{2g}). They have lower energies than the second group. Two are degenerate (d_{xz} and d_{yz} in E_g), and the third (d_{xy} in B_{2g}) has slightly lower energy. In the second group (irreducible

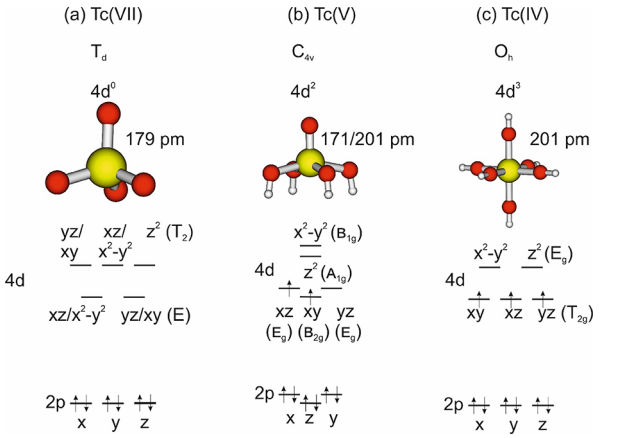

Figure 8. Diagram of energy levels for (a) tetrahedral pertechnetate $[Tc(VII)O_4]^-$, (b) square pyramidal $[Tc(V)O(OH)_4]^-$, and (c) octahedral $[Tc(IV)(OH)_6]^{2}$.

representation A_{1g} and B_{1g}), the orbital energies are significantly higher, but they are not degenerate. The orbital energy of d_{z2} in A_{1g} is slightly lower than the orbital energy of d_{x2-y2} in B_{1g}. The two peaks featured in the XANES spectrum can be assigned to excitations of an additional electron into one of these two groups, either d_{xy}, d_{xz}, and d_{yz} or d_{z2} and d_{x2-y2} (see Figure 8). The states with orbital occupations of both groups are exclusively triplet states ($S = 1$). Figure 9 also clearly shows that many closely spaced transitions contribute to this Tc L_3 edge XANES spectrum.

The experimental Tc L_3 edge XANES spectrum of $[Tc(IV)(OH)_6]^{2-}$ shows only one main peak, which we can very well reproduce with our RASSCF calculations. However, a small shoulder at the higher energy side is visible. In the octahedral ligand field, the 4d orbitals form two groups, d_{xz}, d_{yz}, and d_{xy} in T_{2g} and d_{z2} and d_{x2-y2} in E_g. In the ground state with $S = 3/2$, all three orbitals in T_{2g} are occupied with a parallel spin. The reason for the shape of the L_3 edge XANES spectrum is excitations into these two groups (T_{2g} and E_g) as shown in Figure 9. The two groups of transitions are hardly discernible in the final simulated spectrum (as in the experimental, nearly symmetric WL) because there are so many transitions close in energy. Both groups are a mixture of quartet ($S = 3/2$) and doublet ($S = 1/2$) states. As for $[Tc(V)O(OH)_4]^-$, the $[Tc(IV)(OH)_6]^{2-}$ Tc L_3 edge XANES spectrum is again the sum of many transitions (Figure 9).

Although we were able to accurately reproduce the experimental Tc−O distances observed by Lukens et al. for Tc(IV)−gluconate applying the DFT optimized $[Tc(IV)(GLU_{-2H})_2(OH)_2]^{4-}$ structure, we failed to reproduce the distinct WL splitting into two clearly separated peaks obtained for the Tc L_3 edge XANES spectrum of sample B (cf. Figures 5 and 6). The calculated Tc L_3 edge XANES spectrum based on the $[Tc(IV)(GLU_{-2H})_2(OH)_2]^{4-}$ structure (not shown) only slightly differs from that obtained for $[Tc(IV)(OH)_6]^{2-}$, i.e., exhibiting a broad, nearly symmetric WL resonance.

As mentioned above, the calculated $[Tc(IV)(OH)_6]^{2-}$ and the $[Tc(IV)(GLU_{-2H})_2(OH)_2]^{4-}$ Tc L_3 edge XANES spectra are a convolution of many single transitions. The spectrum of $[Tc(IV)(OH)_6]^{2-}$ in Figure 9 clearly shows two distinct groups of transitions split by about 2 eV in energy forming the overall shape of the spectrum. The same is observed for the $[Tc(IV)(GLU_{-2H})_2(OH)_2]^{4-}$ spectrum (not shown), but the

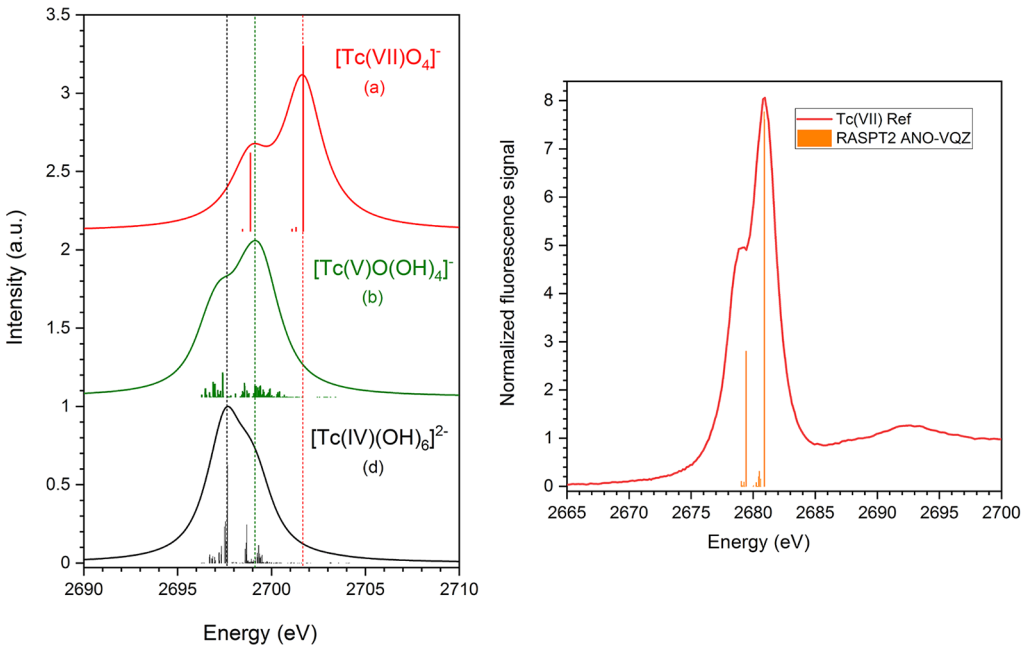

Figure 9. Left panel: ab initio Tc L_3 edge XANES spectra of $[Tc(VII)O_4]^-$, $[Tc(V)O(OH)_4]^-$, and $[Tc(IV)(OH)_6]^{2-}$ (vertically shifted for clarity) obtained by RASSCF/ANO VTZ calculations based on DFT structure optimizations (cf. Figure 7), vertical bars representing transition energies and oscillator strengths of relevant Tc $2p_{3/2} \rightarrow 4d_{5/2}$ excitations and spectral envelopes (solid lines) obtained by convoluting bars with Lorentzians (cf. the text for details). Right panel: ab initio Tc L_3 edge XANES spectra of $[Tc(VII)O_4]^-$ (bars) obtained by RASPT2/ANO VQZ calculations (shifted −4.57 eV) compared to the experimental spectrum (solid line).

calculated splitting between the two groups is not large enough to reproduce the observed Tc L_3 edge XANES spectrum for sample B, which is actually the largest observed in the experiments, cf. (Figures 5 and 6). We conclude for now that in this case, the Tc L_3 edge XANES spectrum depends very critically on the per se unknown molecular structure of the Tc(IV) coordination polyhedron in sample B. Thus, the DFT optimized $[Tc(IV)(GLU_{-2H})_2(OH)_2]^{4-}$ structure might not be close enough to the "real" structure in sample B to reproduce the Tc L_3 edge XANES spectrum. Nevertheless, from the comparison of the three calculated Tc L_3 edge XANES spectra of $[Tc(VII)O_4]^-$, $[Tc(V)O(OH)_4]^-$, and $[Tc(IV)(OH)_6]^{2-}$ in Figure 9 (spectra not shifted with respect to experimental data), it can be clearly seen that the spectra obtained with RASSCF reproduce very well the experimental findings regarding the overall spectral shape and the relative WL positions. This very clearly demonstrates the high quality of our relativistic multireference ab initio calculations and supports the assignment of the observed WL features in the experimental spectra to electronic transitions obtained by our ab initio calculations.

4. DISCUSSION AND CONCLUSIONS

This work highlights the strengths and potential applications of a combined approach including classical wet chemistry methods (measurements of pH, E_h, and [Tc]), advanced spectroscopic techniques (K and L_3 edge XAFS), and theoretical methods (DFT and relativistic multireference ab initio calculations) for the characterization of Tc aqueous samples of relevance in environmental systems or radio pharmaceutical applications, among others.

No reliable chemical and thermodynamic models are available to date for the system Tc−gluconate under reducing conditions.[89] Although attempts based on solubility experiments with TcO_2(am, hyd) are available in the literature,[90,91] the main limitation preventing the development of reliable models is imposed by the yet ill defined redox state and speciation of Tc in the aqueous phase. Our spectroscopic results confirm that gluconate stabilizes Tc in the +V oxidation state under anoxic conditions, but that reduction is further promoted to Tc(IV) under strongly reducing conditions as those imposed by Sn(II). The evaluation of Tc K edge EXAFS data gives relevant insights into structural parameters such as the coordination number and Tc−O distances but does not allow derivation of conclusive chemical models for the Tc(IV)−gluconate complexes prevailing in the aqueous phase. As already hinted in the literature for Tc solid phases,[42,43] our work provides the first evidence on the high sensitivity of L_3 edge XANES toward the molecular environment of Tc in aqueous samples. The coupling of this highly sensitive technique with ab initio methods represents a prominent tool for the accurate characterization of the molecular environment of Tc in the aqueous phase, thus underpinning the development of accurate chemical and thermodynamic models in real aqueous systems. In this aspect, work currently ongoing at KIT INE targets the development of thermodynamic models of Tc in hyperalkaline cementitious systems, in which gluconate is often used as an additive (superplasticizer). This approach can be also considered for a more accurate characterization of Tc in hyperalkaline systems containing gluconate, as those encountered in some of the Hanford waste tanks.[90] The pioneering work of Lukens and co workers on K edge XAFS of the Tc−gluconate system provided relevant insights into the qualitative characterization of this system,[39] which, however, appear insufficient for the development of chemical and thermodynamic models of Tc under these conditions.

The ternary system Tc(VII)−Sn(II)−gluconate has been widely used in the production process of radiopharmaceuticals

labeled with ^{99m}Tc.[4] For this system, it is generally considered that Tc is found in the oxidation state +V.[4,84,92−94] Although this is possibly true in the short equilibration times considered in applications with ^{99m}Tc ($t_{1/2}$ = 6 h) or in systems where Tc(VII) and Sn(II) are present in stoichiometric amounts (1:1), our combined experimental approach confirms that in the presence of an excess of Sn(II) and in the long term ($t \geq$ 400 days), technetium is exclusively found as a soluble Tc(IV)−gluconate aqueous complex.

The successful proof of concept reported in this work for real aqueous samples opens up the application of K and L edge XAFS methods to a large variety of systems. Hence, work planned at KIT INE includes kinetic and thermodynamic studies with Tc L (with L = organic ligands, e.g., gluconate, ISA, EDTA, and citrate) and Tc sulfide systems in reducing conditions, for which the combination of advanced spectroscopic techniques with theoretical calculations is expected to provide key inputs for the assessment of the temporal evolution in the oxidation state of Tc (+VII → +V → +IV) and the definition of correct chemical models, i.e., the complexes governing the aqueous chemistry of technetium. The study of the systems above aims at a fundamental understanding of the stability and coordination chemistry of Tc in reducing systems but has also clear applied implications in the context of nuclear waste disposal, environmental systems, and, to some extent, radiopharmacy.

The present study clearly demonstrates the benefits added by the recent availability of Tc L_3 edge XANES for aqueous Tc specimens in combination with state of the art quantum chemical ab initio methods. While the limited spectral sensitivity and information content (in terms of the three dimensional arrangement of coordinating ligand atoms) of the conventional K edge fingerprinting method may lead to ambiguity in the interpretation of XAFS data, the direct probe of Tc 4d states involved in ligand bonding enables a precise differentiation of Tc species with formally identical oxidation states. However, any satisfactory reproduction of experimental Tc L_3 edge XANES features based on RASSCF/RASPT2 calculations critically depends on the determination of the correct coordination polyhedron—an open issue still to be solved in the case of the Tc(IV)−gluconate complex (sample B) investigated in this study.

■ ASSOCIATED CONTENT

● Supporting Information

The Supporting Information is available free of charge at https://pubs.acs.org/doi/10.1021/acs.inorgchem.1c01487.

(Section A) Detailed description of the thermodynamic data currently available for Tc; (Section B) comprehensive review of Tc K edge XAFS results available in the literature since the 1980s (PDF)

■ AUTHOR INFORMATION

Corresponding Author

Jörg Rothe − *Karlsruhe Institute of Technology (KIT), Institute for Nuclear Waste Disposal (INE), D 76021 Karlsruhe, Germany;* orcid.org/0000 0001 5366 2129; Email: joerg.rothe@kit.edu

Authors

Kathy Dardenne − *Karlsruhe Institute of Technology (KIT), Institute for Nuclear Waste Disposal (INE), D 76021 Karlsruhe, Germany*

Sarah Duckworth − *Karlsruhe Institute of Technology (KIT), Institute for Nuclear Waste Disposal (INE), D 76021 Karlsruhe, Germany*

Xavier Gaona − *Karlsruhe Institute of Technology (KIT), Institute for Nuclear Waste Disposal (INE), D 76021 Karlsruhe, Germany*

Robert Polly − *Karlsruhe Institute of Technology (KIT), Institute for Nuclear Waste Disposal (INE), D 76021 Karlsruhe, Germany*

Bernd Schimmelpfennig − *Karlsruhe Institute of Technology (KIT), Institute for Nuclear Waste Disposal (INE), D 76021 Karlsruhe, Germany*

Tim Pruessmann − *Karlsruhe Institute of Technology (KIT), Institute for Nuclear Waste Disposal (INE), D 76021 Karlsruhe, Germany;* orcid.org/0000 0002 7903 9199

Marcus Altmaier − *Karlsruhe Institute of Technology (KIT), Institute for Nuclear Waste Disposal (INE), D 76021 Karlsruhe, Germany*

Horst Geckeis − *Karlsruhe Institute of Technology (KIT), Institute for Nuclear Waste Disposal (INE), D 76021 Karlsruhe, Germany*

Notes

The authors declare no competing financial interest.

■ ACKNOWLEDGMENTS

This work was partly funded by the German Ministry of Economic Affairs and Energy (BMWi) within the framework of the VESPA II project (contract number 02E11607C). We acknowledge the KIT light source for provision of beamtime at the INE and ACT Beamlines operated by the Institute for Nuclear Waste Disposal, and we would like to thank the Institute for Beam Physics and Technology (IBPT) for the operation of the storage ring, the Karlsruhe Research Accelerator (KARA). K. Hardock is acknowledged for preparing the 3D CAD drawings of the He flow cell setup and F. Holl and V. Krepper for the design and manufacturing. Dr. Bernd Schimmelpfennig passed away during the preparation of this manuscript. Theoretical calculations presented in Section 3.3 have been significantly inspired by his late work. W.W. Lukens (Lawrence Berkeley National Laboratory) is kindly acknowledged for fruitful discussions and for sharing unpublished data on the Tc gluconate system.

■ ADDITIONAL NOTE

[a]This complex is quoted as Tc(gluconate)$_2^{2-}$ in the original publication.

■ REFERENCES

(1) Icenhower, J. P.; Qafoku, N. P.; Zachara, J. M.; Martin, W. J. The Biogeochemistry of Technetium: A Review of the Behavior of an Artificial Element in the Natural Environment. *Am. J. Sci.* **2010**, *310*, 721−752.

(2) Darab, J. G.; Smith, P. A. Chemistry of technetium and rhenium species during low level radioactive waste vitrification. *Chem. Mater.* **1996**, *8*, 1004−1021.

(3) Gephart, R. E. A short history of waste management at the Hanford Site. *Phys. Chem. Earth* **2010**, *35*, 298−306.
(4) Mazzi, U., S. R, Pietzsch, H.J., Künstler, J.U., Spies, H., Technetium in Medicine. In *Technetium 99m Pharmaceuticals*; I.Z, Ed. Springer: Berlin, Heidelberg, 2007, DOI: 10.1007/978 3 540 33990 8 2.
(5) Andros, G.; Harper, P. V.; Lathrop, K. A.; Mccardle, R. J. Pertechnetate 99m Localization in Man with Applications to Thyroid Scanning and Study of Thyroid Physiology. *J. Clin. Endocrinol. Metab.* **1965**, *25*, 1067.
(6) Mcafee, J. G.; Stern, H. S.; Fueger, G. F.; Baggish, M. S.; Holzman, G. B.; Zolle, I. Tc 99m Labeled Serum Albumin for Scintillation Scanning of the Placenta. *J. Nucl. Med.* **1964**, *5*, 936−946.
(7) Stern, H. S.; Mcafee, J. G.; Subramanian, G. Preparation Distribution and Utilization of Technetium 99m Sulfur Colloid. *J. Nucl. Med.* **1966**, *7*, 665−675.
(8) Liu, S.; Edwards, D. S. Tc 99m Labeled small peptides as diagnostic radiopharmaceuticals. *Chem. Rev.* **1999**, *99*, 2235−2268.
(9) Mendez Rojas, M. A.; Kharisov, B. I.; Tsivadze, A. Y. Recent advances on technetium complexes: coordination chemistry and medical applications. *J. Coord. Chem.* **2006**, *59*, 1−63.
(10) Rard, J. A.; Rand, M.; Anderegg, G.; Wanner, H. *Chemical Thermodynamics Vol. 3. Chemical Thermodynamics of Technetium*; Elsevier: North Holland, Amsterdam, 1999.
(11) Schwochau, K. *Technetium chemistry and radiopharmaceutical applications*; Wiley VCH: Weinheim, 2000; p 446S.
(12) German, K. E.; Obruchnikova, Y. A.; Safonov, A. V.; Tregubova, V. E.; Afanas'ev, A. V.; Kopytin, A. V.; Kryzhovets, O. S.; Poineau, F.; Abkhalimov, E. V.; Shiryaev, A. A. Kinetics of the formation of precipitates and the physicochemical properties of technetium 99 and rhenium sulfides according to small angle X ray scattering and ultramicrocentrifugation data. *Russ. J. Inorg. Chem.* **2016**, *61*, 1445−1450.
(13) Pearce, C. I.; Icenhower, J. P.; Asmussen, R. M.; Tratnyek, P. G.; Rosso, K. M.; Lukens, W. W.; Qafoku, N. P. Technetium Stabilization in Low Solubility Sulfide Phases: A Review. *Acs Earth Space Chem.* **2018**, *2*, 532−547.
(14) Zolle, I., *Technetium 99m pharmaceuticals preparation and quality control in nuclear medicine; with 29 tables*; Springer: Berlin, 2007; p 345 S.
(15) Kissel, G.; Feldberg, S. W. Disproportionation of Technetate Ion in Aqueous Alkaline Media. An Electrochemical Study. *J. Phys. Chem.* **1969**, *73*, 3082.
(16) Deutsch, E.; Heineman, W. R.; Hurst, R.; Sullivan, J. C.; Mulac, W. A.; Gordon, S. Production, Detection, and Characterization of Transient Hexavalent Technetium in Aqueous Alkaline Media by Pulse Radiolysis and Very Fast Scan Cyclic Voltammetry. *J. Chem. Soc. Chem. Commun.* **1978**, *23*, 1038−1040.
(17) Founta, A.; Aikens, D. A.; Clark, H. M. Mechanism and Kinetics of the Stepwise Voltammetric Reduction of Pertechnetate in Alkaline Solution to Tc(Vi), Tc(V) and Tc(Iv). *J. Electroanal. Chem.* **1987**, *219*, 221−246.
(18) Bratu, C.; Bratu, G.; Galateanu, I.; Roman, M. Study of Lower Valence States of Technetium. *J. Radioanal. Chem.* **1975**, *26*, 5−16.
(19) Grassi, J.; Devynck, J.; Tremillon, B. Electrochemical Studies of Technetium at a Mercury Electrode. *Anal. Chim. Acta* **1979**, *107*, 47−58.
(20) Nicholson, T.; Kramer, D. J.; Davison, A.; Jones, A. G. Synthesis and characterization of a technetium nitrido dimer. *Inorg. Chim. Acta* **2001**, *316*, 110−112.
(21) Baldas, J.; Colmanet, S. F.; Williams, G. A. Preparation of the Technetium(Vi) Aquanitrido Complexes (Net4)[Tcnx4(Oh2)] (X = Cl or Br) Crystal Structures of (Net4)[Tcnbr4(Oh2)] and Cs2[Tcncl5]. *Inorg. Chim. Acta* **1991**, *179*, 189−194.
(22) Baldas, J.; Boas, J. F.; Colmanet, S. F.; Ivanov, Z.; Williams, G. A. Monomer, μ Oxo Dimer, Di(μ Oxo) Dimer Interconversion of Nitridotechnetium(Vi) Complexes in Solution. *Radiochim. Acta* **1993**, *63*, 111−116.
(23) Balasekaran, S. M.; Hagenbach, A.; Abram, U. Tetrafluoridonitridotechnetate(VI) Reactions and Structures. *Z Anorg Allg Chem* **2018**, *644*, 1158−1163.
(24) Mazzi, U. The Coordination Chemistry of Technetium in Its Intermediate Oxidation States. *Polyhedron* **1989**, *8*, 1683−1688.
(25) Spies, H.; Johannsen, B. Preparation and Characterization of Tetraethylammonium Bis(1,2 Dicyanoethylenedithiolato) Oxotechnetate(V). *Inorg. Chim. Acta* **1979**, *33*, L113−L113.
(26) Bandoli, G.; Mazzi, U.; Abram, U.; Spies, H.; Munze, R. Synthesis and X Ray Crystal Structure of Tetraethylammonium Bis(1,1 Dicyanoethene 2,2 Diselenolato)Oxotechnetate(V), [Et4n][Tco(Se2c=C(Cn)2)2]. *Polyhedron* **1987**, *6*, 1547−1550.
(27) Guillaumont, R.; Fanghänel, J.; Neck, V.; Fuger, J.; Palmer, D. A.; Grenthe, I.; Rand, M. H., *Chemical Thermodynamics Vol. 5. Update on the Chemical Thermodynamics of Uranium, Neptunium, Plutonium, Americium and Technetium*; Elsevier, North Holland: Amsterdam, 2003.
(28) Chotkowski, M.; Czerwinski, A. Thin layer spectroelectro chemical studies of pertechnetate reduction on the gold electrodes in acidic media. *Electrochim. Acta* **2014**, *121*, 44−48.
(29) Poineau, F.; Fattahi, M.; Den Auwer, C.; Hennig, C.; Grambow, B. Speciation of technetium and rhenium complexes by in situ XAS electrochemistry. *Radiochim. Acta* **2006**, *94*, 283−289.
(30) Seifert, S.; Noll, B.; Munze, R. Studies of the Complex Formation of Technetium(Iv) with Aminopolycarboxylic Acids in Aqueous Solution. *Int. J. Appl. Radiat. Isot.* **1982**, *33*, 1393−1398.
(31) Gonzalez, R.; Kremer, C.; Chiozzone, R.; Torres, J.; Rivero, M.; Leon, A.; Kremer, E. Preparation and chemical studies on Tc(III) complexes containing polyaminocarboxylic acids. *Radiochim. Acta* **1998**, *81*, 207−214.
(32) Barrera, J.; Burrell, A. K.; Bryan, J. C. Technetium(III), technitium(II), and technetium(I) complexes with pyridine ligands. Can pyridine coordination stabilize the low oxidation states of technetium? *Inorg. Chem.* **1996**, *35*, 335−341.
(33) Archer, C. M.; Dilworth, J. R.; Kelly, J. D.; Mcpartlin, M. The Synthesis and Structure of a Technetium Nitride Cation and Tetrabromotechnetate(Ii) Anion in $[Tcbr(N)(Bipy)_2]_2[Tcbr_4]$ (Bipy = 2,2' Bipyridyl). *J. Chem. Soc. Chem. Commun.* **1989**, *6*, 375−376.
(34) Seifert, S.; Muenze, R.; Leibnitz, P.; Reck, G.; Stach, J. Preparation, Characterization and Crystal Structure of a Mixed Ligand Complex of Technetium with Dppe and Oxalic Acid Oxalato Bis(1,2 Bis(Diphenylphosphino)Ethane)Technetium(Ii). *Inorg. Chim. Acta* **1992**, *193*, 167−172.
(35) Gong, C. M. S.; Lukens, W. W.; Poineau, F.; Czerwinski, K. R. Reduction of pertechnetate by acetohydroxamic acid: Formation of [Tc II(NO)(AHA)(2)(H2O)](+) and implications for the UREX process. *Inorg. Chem.* **2008**, *47*, 6674−6680.
(36) Alberto, R.; Schibli, R.; Egli, A.; Schubiger, A. P.; Abram, U.; Kaden, T. A. A novel organometallic aqua complex of technetium for the labeling of biomolecules: Synthesis of $[^{99m}Tc\ (OH_2)_3(CO)_3]^+$ from $[^{99m}Tc\ (TcO_4)^-]^-$ in aqueous solution and its reaction with a bifunctional ligand. *J. Am. Chem. Soc.* **1998**, *120*, 7987−7988.
(37) Hayes, T. R.; Kasten, B. B.; Barnes, C. L.; Benny, P. D. Rhenium and technetium bi and tricarbonyl complexes in a new strategy for biomolecule incorporation using click chemistry dagger. *Dalton Trans.* **2014**, *43*, 6998−7001.
(38) Lukens, W. W.; Bucher, J. J.; Edelstein, N. M.; Shuh, D. K. Products of pertechnetate radiolysis in highly alkaline solution: Structure of TcO_2 center dot xH_2O. *Environ. Sci. Technol.* **2002**, *36*, 1124−1129.
(39) Lukens, W. W.; Shuh, D. K.; Schroeder, N. C.; Ashley, K. R. Identification of the non pertechnetate species in Hanford waste tanks, Tc(I) carbonyl complexes. *Environ. Sci. Technol.* **2004**, *38*, 229−233.
(40) Chatterjee, S.; Hall, G. B.; Engelhard, M. H.; Du, Y. G.; Washton, N. M.; Lukens, W. W.; Lee, S.; Pearce, C. I.; Levitskaia, T. G. Spectroscopic Characterization of Aqua $[fac\ Tc(CO)_3]^+$ Com plexes at High Ionic Strength. *Inorg. Chem.* **2018**, *57*, 6903−6912.

(41) Krause, M. O.; Oliver, J. H. Natural Widths of Atomic K Levels and L Levels,K α X Ray Lines and Several Kll Auger Lines. *J. Phys. Chem. Ref. Data* **1979**, *8*, 329−338.
(42) Blanchard, P. E. R.; Reynolds, E.; Kennedy, B. J.; Ling, C. D.; Zhang, Z.; Thorogood, G.; Cowie, B. C. C.; Thomsen, L. An unconventional method for measuring the Tc L 3 edge of technetium compounds. *J. Synchrotron Radiat.* **2014**, *21*, 1275−1281.
(43) Bauters, S.; Scheinost, A. C.; Schmeide, K.; Weiss, S.; Dardenne, K.; Rothe, J.; Mayordomo, N.; Steudtner, R.; Stumpf, T.; Abram, U.; Butorin, S. M.; Kvashnina, K. O. Signatures of technetium oxidation states: a new approach. *Chem. Commun.* **2020**, *56*, 9608−9611.
(44) Rothe, J.; Butorin, S.; Dardenne, K.; Denecke, M. A.; Kienzler, B.; Loble, M.; Metz, V.; Seibert, A.; Steppert, M.; Vitova, T.; Walther, C.; Geckeis, H. The INE Beamline for actinide science at ANKA. *Rev. Sci. Instrum.* **2012**, *83*, No. 043105.
(45) Altmaier, M.; Metz, V.; Neck, V.; Müller, R.; Fanghänel, T. Solid liquid equilibria of $Mg(OH)_2$(cr) and $Mg_2(OH)_3Cl\ 4H_2O$(cr) in the system Mg Na H OH O Cl H_2O at 25 degrees C. *Geochim. Cosmochim. Acta* **2003**, *67*, 3595−3601.
(46) Grenthe, I.; Stumm, W.; Laaksuharju, M.; Nilsson, A. C.; Wikberg, P. Redox potentials and redox reactions in deep ground water systems. *Chem. Geol.* **1992**, *98*, 131−150.
(47) Altmaier, M.; Gaona, X.; Fellhauer, D.; Buckau, G. *Intercomparison of redox determination methods on designed and near neutral aqueous systems*; KIT SR 7572; Karlsruhe Institute of Technology: Karlsruhe, 2010; p 34.
(48) Neck, V.; Altmaier, M.; Fanghänel, T. Solubility of plutonium hydroxides/hydrous oxides under reducing conditions and in the presence of oxygen. *C. R. Chim.* **2007**, *10*, 959−977.
(49) Zimina, A.; Dardenne, K.; Denecke, M. A.; Doronkin, D. E.; Huttel, E.; Lichtenberg, H.; Mangold, S.; Pruessmann, T.; Rothe, J.; Spangenberg, T.; Steininger, R.; Vitova, T.; Geckeis, H.; Grunwaldt, J. D. CAT ACT A new highly versatile x ray spectroscopy beamline for catalysis and radionuclide science at the KIT synchrotron light facility ANKA. *Rev. Sci. Instrum.* **2017**, *88*, 113113.
(50) Vitova, T.; Pidchenko, I.; Fellhauer, D.; Pruessmann, T.; Bahl, S.; Dardenne, K.; Yokosawa, T.; Schimmelpfennig, B.; Altmaier, M.; Denecke, M.; Rothe, J.; Geckeis, H. Exploring the electronic structure and speciation of aqueous and colloidal Pu with high energy resolution XANES and computations. *Chem. Commun.* **2018**, *54*, 12824−12827.
(51) Breinig, M.; Chen, M. H.; Ice, G. E.; Parente, F.; Crasemann, B.; Brown, G. S. Atomic Inner Shell Level Energies Determined by Absorption Spectrometry with Synchrotron Radiation. *Phys. Rev. A* **1980**, *22*, 520−528.
(52) Josefsson, I.; Kunnus, K.; Schreck, S.; Fohlisch, A.; de Groot, F.; Wernet, P.; Odelius, M. Ab Initio Calculations of X ray Spectra: Atomic Multiplet and Molecular Orbital Effects in a Multiconfigura tional SCF Approach to the L Edge Spectra of Transition Metal Complexes. *J. Phys. Chem. Lett.* **2012**, *3*, 3565−3570.
(53) Pinjari, R. V.; Delcey, M. G.; Guo, M.; Odelius, M.; Lundberg, M. Restricted active space calculations of L edge x ray absorption spectra: From molecular orbitals to multiplet states. *J. Chem. Phys.* **2014**, *141*, 124116.
(54) Pinjari, R. V.; Delcey, M. G.; Guo, M.; Odelius, M.; Lundberg, M. Cost and sensitivity of restricted active space calculations of metal L edge X ray absorption spectra. *J. Comput. Chem.* **2016**, *37*, 477−486.
(55) Norman, P.; Dreuw, A. Simulating X ray Spectroscopies and Calculating Core Excited States of Molecules. *Chem. Rev.* **2018**, *118*, 7208−7248.
(56) Bokarev, S. I.; Kuhn, O. Theoretical X ray spectroscopy of transition metal compounds. *WIREs Comput. Mol. Sci.* **2020**, *10*, e1433.
(57) Lundberg, M.; Delcey, M. G., Multiconfigurational Approach to X ray Spectroscopy of Transition Metal Complexes. In *Transition Metals in Coordination Environments: Computational Chemistry and Catalysis Viewpoints*, Broclawik, E.; Borowski, T.; Radoó, M., Eds. Springer International Publishing: Cham, 2019; pp. 185−217, DOI: 10.1007/978 3 030 11714 6 7.
(58) Schafer, A.; Horn, H.; Ahlrichs, R. Fully Optimized Contracted Gaussian Basis Sets for Atoms Li to Kr. *J. Chem. Phys.* **1992**, *97*, 2571−2577.
(59) Eichkorn, K.; Treutler, O.; Öhm, H.; Haser, M.; Ahlrichs, R. Auxiliary Basis Sets to Approximate Coulomb Potentials. *Chem. Phys. Lett.* **1995**, *242*, 652−660.
(60) Treutler, O.; Ahlrichs, R. Efficient Molecular Numerical Integration Schemes. *J. Chem. Phys.* **1995**, *102*, 346−354.
(61) Eichkorn, K.; Weigend, F.; Treutler, O.; Ahlrichs, R. Auxiliary basis sets for main row atoms and transition metals and their use to approximate Coulomb potentials. *Theor. Chem. Acc.* **1997**, *97*, 119−124.
(62) von Arnim, M.; Ahlrichs, R. Geometry optimization in generalized natural internal coordinates. *J Chem Phys* **1999**, *111*, 9183−9190.
(63) Deglmann, P.; May, K.; Furche, F.; Ahlrichs, R. Nuclear second analytical derivative calculations using auxiliary basis set expansions. *Chem. Phys. Lett.* **2004**, *384*, 103−107.
(64) Weigend, F.; Haser, M.; Patzelt, H.; Ahlrichs, R. RI MP2: optimized auxiliary basis sets and demonstration of efficiency. *Chem. Phys. Lett.* **1998**, *294*, 143−152.
(65) Weigend, F.; Ahlrichs, R. Balanced basis sets of split valence, triple zeta valence and quadruple zeta valence quality for H to Rn: Design and assessment of accuracy. *Phys. Chem. Chem. Phys.* **2005**, *7*, 3297−3305.
(66) Andrae, D.; Haussermann, U.; Dolg, M.; Stoll, H.; Preuss, H. Energy Adjusted Abinitio Pseudopotentials for the 2nd and 3rd Row Transition Elements. *Theor. Chim. Acta* **1990**, *77*, 123−141.
(67) Aquilante, F.; Autschbach, J.; Carlson, R. K.; Chibotaru, L. F.; Delcey, M. G.; De Vico, L.; Galvan, I. F.; Ferre, N.; Frutos, L. M.; Gagliardi, L.; Garavelli, M.; Giussani, A.; Hoyer, C. E.; Li Manni, G.; Lischka, H.; Ma, D. X.; Malmqvist, P. A.; Muller, T.; Nenov, A.; Olivucci, M.; Pedersen, T. B.; Peng, D. L.; Plasser, F.; Pritchard, B.; Reiher, M.; Rivalta, I.; Schapiro, I.; Segarra Marti, J.; Stenrup, M.; Truhlar, D. G.; Ungur, L.; Valentini, A.; Vancoillie, S.; Veryazov, V.; Vysotskiy, V. P.; Weingart, O.; Zapata, F.; Lindh, R. Molcas 8: New capabilities for multiconfigurational quantum chemical calculations across the periodic table. *J. Comput. Chem.* **2016**, *37*, 506−541.
(68) Malmqvist, P. A.; Rendell, A.; Roos, B. O. The Restricted Active Space Self Consistent Field Method, Implemented with a Split Graph Unitary Group Approach. *J. Phys. Chem.* **1990**, *94*, 5477−5482.
(69) Malmqvist, P. Å.; Pierloot, K.; Shahi, A. R. M.; Cramer, C. J.; Gagliardi, L. The restricted active space followed by second order perturbation theory method: Theory and application to the study of CuO_2 and Cu_2O_2 systems. *J. Chem. Phys.* **2008**, *128*, 204109.
(70) Malmqvist, P. Å.; Roos, B. O.; Schimmelpfennig, B. The restricted active space (RAS) state interaction approach with spin orbit coupling. *Chem. Phys. Lett.* **2002**, *357*, 230−240.
(71) Roos, B. O.; Lindh, R.; Malmqvist, P. Å.; Veryazov, V.; Widmark, P. O. Main group atoms and dimers studied with a new relativistic ANO basis set. *J. Phys. Chem. A* **2004**, *108*, 2851−2858.
(72) Roos, B. O.; Lindh, R.; Malmqvist, P. Å.; Veryazov, V.; Widmark, P. O. New relativistic ANO basis sets for transition metal atoms. *J. Phys. Chem. A* **2005**, *109*, 6575−6579.
(73) Kobayashi, T.; Scheinost, A. C.; Fellhauer, D.; Gaona, X.; Altmaier, M. Redox behavior of Tc(VII)/Tc(IV) under various reducing conditions in 0.1 M NaCl solutions. *Radiochim. Acta* **2013**, *101*, 323−332.
(74) Yalçintaş, E.; Gaona, X.; Altmaier, M.; Dardenne, K.; Polly, R.; Geckeis, H. Thermodynamic description of Tc(IV) solubility and hydrolysis in dilute to concentrated NaCl, $MgCl_2$ and $CaCl_2$ solutions. *Dalton Trans.* **2016**, *45*, 8916−8936.
(75) Yalçintaş, E.; Gaona, X.; Scheinost, A. C.; Kobayashi, T.; Altmaier, M.; Geckeis, H. Redox chemistry of Tc(VII)/Tc(IV) in dilute to concentrated NaCl and $MgCl_2$ solutions. *Radiochim. Acta* **2015**, *103*, 57−72.

(76) Baumann, A.; Yalcintas, E.; Gaona, X.; Altmaier, M.; Geckeis, H. Solubility and hydrolysis of Tc(IV) in dilute to concentrated KCl solutions: an extended thermodynamic model for Tc^{4+} H^+ K^+ Na^+ Mg^{2+} Ca^{2+} OH^- Cl^- $H_2O(l)$ mixed systems. *New J. Chem.* **2017**, *41*, 9077−9086.
(77) Colmanet, S. F.; Williams, G. A.; Mackay, M. F. Preparation and Crystal Structures of Bis(Tetraphenylarsonium) Tris(Oxalato) Technetate(IV), and Tetraphenylarsonium Tris(Benzene 1,2 Dithiolato)Technetate(V): Octahedral Versus Trigonal Prismatic Geometry for Tris Bidentate Complexes of Technetium. *J. Chem. Soc., Dalton Trans.* **1987**, *10*, 2305−2310.
(78) Buergi, H. B.; Anderegg, G.; Blauenstein, P. Preparation, Characterization, and Crystal, Molecular, and Electronic Structure of (H2edta)Tc 99(IV)(Mu O)2tC 99(IV)(H2edta).5h2O A2.33 A Tc Tc Distance Which May Represent a Sigma 2 Pi 2 Delta Star 2 Bond. *Inorg. Chem.* **1981**, *20*, 3829−3834.
(79) Davison, A.; Depamphilis, B. V.; Jones, A. G.; Franklin, K. J.; Lock, C. J. L. Synthesis and Characterization of Complexes Containing the Bis(1,2 Diolato) Oxotechnetium(V) Core. *Inorg. Chim. Acta* **1987**, *128*, 161−167.
(80) Baldas, J.; Colmanet, S. F.; Mackay, M. F. Preparation and Crystal Structures of [Asph4]4[Tc4n4o2(Ox)6] and [Asph4]2[Tco (Ox)2(Hox)].3h2O Technetium Complexes Containing Quadriden tate or Unidentate Oxalato Ligands. *J. Chem. Soc., Dalton Trans.* **1988**, *7*, 1725−1731.
(81) Spies, H.; Johannsen, B.; Munze, R.; Unverferth, K. Kinetic Investigations on the Reaction of Technetium(V) Gluconate with Meso Dimercaptosuccinic Acid and Meso Dimercaptosuccinic Acid Dimethylester. *Radiochem. Radioanal. Lett.* **1980**, *43*, 311−318.
(82) Spies, H.; Johannsen, B. Oxotechnetium(V)Bis(Dithiolato) Complexes. *Inorg. Chim. Acta* **1981**, *48*, 255−258.
(83) Russell, C. D.; Speiser, A. G. Complexes of Technetium with Hydroxycarboxylic Acids Gluconic, Glucoheptonic, Tartaric, and Citric. *J. Nucl. Med.* **1980**, *21*, 1086−1090.
(84) Hwang, L. L. Y.; Ronca, N.; Solomon, N. A.; Steigman, J. Complexes of Technetium with Polyhydric Ligands. *Int. J. Appl. Radiat. Isot.* **1985**, *36*, 475−480.
(85) Steigman, J.; Meinken, G.; Richards, P. Reduction of Pertechnetate 99 by Stannous Chloride I. Stoichiometry of Reaction in HCl, in a Citrate Buffer and in a Dtpa Buffer. *Int. J. Appl. Radiat. Isot.* **1975**, *26*, 601−609.
(86) Burton Pye, B. P.; Dembowski, M.; Lukens, W. W.; Cruz, A.; Althour, A.; Lopez, G. E.; Salcedo, R.; Gallagher, C. M. B.; McGregor, D.; Francesconi, L. C. Synthesis and Characterization of Non Aqueous $[Tc\ ^{x}M\ PW11O39]^{n-}$ with M = O, N: Comparing Tc^{V} and Tc^{VI} in Metal Oxide Matrices. *Eur. J. Inorg. Chem.* **2019**, *2019*, 4826−4834.
(87) Baumann, A.; Yalçintaş, E.; Gaona, X.; Polly, R.; Dardenne, K.; Prussmann, T.; Rothe, J.; Altmaier, M.; Geckeis, H. Thermodynamic description of Tc(IV) solubility and carbonate complexation in alkaline $NaHCO_3$ Na_2CO_3 NaCl systems. *Dalton Trans.* **2018**, *47*, 4377−4392.
(88) Weaver, J.; Soderquist, C. Z.; Washton, N. M.; Lipton, A. S.; Gassman, P. L.; Lukens, W. W.; Kruger, A. A.; Wall, N. A.; McCloy, J. S. Chemical Trends in Solid Alkali Pertechnetates. *Inorg. Chem.* **2017**, *56*, 2533−2544.
(89) Hummel, W.; Anderegg, G.; Rao, L.; Puigdomènech, I.; Tochiyama, O., *Chemical Thermodynamics of Compounds and Complexes of U, Np, Pu, Am, Tc, Se, Ni and Zr with Selected Organic Ligands*. Elsevier: Amsterdam, 2005.
(90) Hess, N.; Xia, Y.; Felmy, A. R., Solubility of $TcO_2{\cdot}xH_2O(am)$ in the presence of gluconate in aqueous solution. In *Nuclear Waste Management*; Wang, P., Ed. American Chemical Society: Washington DC, 2006.
(91) Evans, N.; Hallam, R.; Aldridge, S.; Warwick, P.; Bryan, N. In *The complexation of Tc(IV) with gluconic acid at high pH*; 2008.
(92) Steigman, J.; Hwang, L.; Srivastava, S. Complexes of Reduced Tc 99 with Polyhydric Compounds. *J. Labelled Compd. Radiopharm.* **2006**, *943*, 286−301.
(93) Hwang, L. L. Y.; Ronca, N.; Solomon, N. A.; Steigman, J. Extraction of Tc(V) from Radiopharmaceuticals. *Int. J. Appl. Radiat. Isot.* **1984**, *35*, 825−830.
(94) Dekieviet, W. Technetium Radiopharmaceuticals Chemical Characterization and Tissue Distribution of Tc Glucoheptonate Using Tc 99m and Carrier Tc 99. *J. Nucl. Med.* **1981**, *22*, 703−709.